2

UCID- 16664

LAWRENCE LIVERMORE LABORATORY

University of California/Livermore, California

INSTABILITY-THRESHOLD DATA FROM THE BASEBALL II VACUUM-BUILDUP EXPERIMENT

James H. Foote

December 30, 1974

Prepared for U. S. Atomic Energy Commission under contract no. W-7405-Eng-48

DISCLAIMER

CONTENTS

INSTABILITY-THRESHOLD DATA FROM THE BASEBALL II VACUUM-BUILDUP EXPERIMENT*

James H. Foote

Lawrence Livermore Laboratory, University of California

Livermore, California

ABSTRACT

The instability-threshold data from the Baseball II vacuum-buildup experiment are now extensive, and the parameter range covered by these measurements is large. The agreement with the Baseball I threshold results is poor. Although some of the thresholds lie near the Baseball I average-threshold line and its extension on an $\varepsilon = (\omega_{pi}/\omega_{ci})^2$ vs $e\phi/W_i$ plot, many fall considerably below. The large spread in the data, when plotted in this way, is well outside the estimated experimental uncertainty. The data scatter evidently is not due to gross inaccuracies in our measurements: a plot of the combined Baseball I and Baseball II threshold data shows a strong and reasonably well-defined variation of density with plasma potential. This variation is apparently a manifestation of the classical collisional relations, which must be satisfied even for instability-threshold data. Selected sets of Baseball II threshold data, obtained when experimental conditions were held almost constant except for one particular parameter, show a strong variation of ε with $e\phi/W_i$. This variation is in agreement with the classical equations but in disagreement with the Baseball I ion-cyclotron-instability theory. There is no satisfactory explanation for the Baseball II threshold

data at this time. The quantity $e\phi/W_i$ appears to be no longer the controlling parameter for the instability. However, the threshold and maximum (instability-limited) densities do seem to vary approximately as the square of the magnetic-field magnitude, indicating that ε $(\propto n_i/B^2)$ is still important.

*Work performed under the auspices of the U.S. Atomic Energy Commision.

I. Introduction

An extensive series of measurements on the threshold for the instability observed in the Baseball I (BBI) experiment has been previously reported.[1] There, the experimental threshold results were interpreted in terms of an ion-cyclotron instability with Landau damping of electron-plasma waves in the body of the plasma. The pertinent parameters in that theory are $\varepsilon = (\omega_{pi}/\omega_{ci})^2 \left[\propto n_i M/B^2\right]$ and $e\phi/W_i$, where ω_{pi} and ω_{ci} are the ion plasma and cyclotron frequencies, respectively, n_i is the peak ion density, M is the ion mass, B is the magnetic-field magnitude, ϕ is the plasma potential, and W_i, the ion energy. The BBI theory predicts that the threshold values should give an $\varepsilon \propto e\phi/W_i$ variation. The BBI results do seem to follow this behavior, on the average, and thus define a 45-deg line on an ε vs $e\phi/W_i$ log-log plot.

It was assumed that the same instability would be observed in Baseball II (BBII). Lower ion energies were emphasized in this later experiment in the expectation that a scattered ion distribution would raise the instability-threshold level, i.e., that the experimental threshold points would eventually rise above the BBI 45-deg line. It was hoped that a higher and more interesting density regime could be reached in this way.

The BBII results are not as expected. The numerous instability-threshold measurements now available have a large scatter on an ε vs $e\phi/W_i$ plot, none is above the BBI average-threshold line, and many are considerably below. Even those measurements taken under the best BBII conditions, where considerable ion scattering was evidently occurring, fall low. We cannot explain these results at this time.

This report summarizes the BBII threshold data. In Sec. II we present the data and the manner in which they were obtained. The classical collisional equations have been used to check the accuracy of the measurements, as discussed in Sec. III. We summarize the BBI instability theory in Sec. IV, and try to apply it to the BBII threshold data. Some concluding and summarizing remarks are made in Sec. V.

II. Instability-Threshold Data

Figure 1 shows many of the BBII instability-threshold measurements on an ϵ vs $e\phi/W_i$ plot, demonstrating the large variation obtained in the experimental parameters at threshold. The points plotted are a general sample of the array of BBII threshold measurements presented in this report (for the full array, see Table I). A display of all the data would have resulted in too much overlapping and a resulting loss of clarity in the presentation. The average-threshold 45-deg line obtained in the BBI analysis is reproduced in this figure and extended further upward, to provide a comparison with the earlier work.

Threshold for a given set of conditions is defined as that value of ϵ at which, as the plasma density is increased, definite sharp bursts of fast ($\geq$300 eV) ions out the mirrors begin to appear. Somewhat above threshold, bursts of activity with frequencies in the range of the ion-cyclotron frequency also begin to be detectable. In the vicinity of a given threshold, we usually adjust the neutral-beam intensity to vary the plasma density and thus determine the threshold level: raising the beam above the threshold level increases ε and the bursting activity, while lowering the beam level decreases ε, and essentially no fast-ion spikes are then observed. Thus, in Fig. 1, the region above the plotted threshold values has been labeled unstable, and the region below, quiescent.

Four experimental quantities are needed to plot a threshold point in Fig. 1: n_i, B, ϕ, and W_i. Values of the peak density n_i are obtained from measured values of the average line or volume density by applying a conversion factor, assumed approximately constant for all the threshold data. A double-pass 17-GHz microwave-interferometer measurement gives the average density over the microwave path through the plasma. The diameter of the plasma is assumed to be 20 cm for this calculation. For the lower threshold points in Fig. 1, microwave-interferometer density measurements were not always possible. There, relative values of $(nT_e)/\phi$ are used, normalized to the microwave readings at higher densities. The quantity (nT_e) is determined from a signal emitted by the plasma at the electron-cyclotron frequency, the amplitude of which is proportional to the product of the electron density and the electron temperature. We assume that $kT_e \propto e\phi$ over a limited range of ϕ, so that we can eliminate the T_e variation by dividing by ϕ.* Values of ϕ used here and in $e\phi/W_i$ are obtained from a

*The plasma potential ϕ and the corresponding energy $e\phi$, acquired by a singly charged positive ion escaping the plasma region and thus falling through the potential difference ϕ, are used almost interchangeably in this report.

retarding-grid analyzer positioned on or near the magnetic axis considerably outside the mirror. The plasma potential is defined as equivalent to the bias necessary to stop essentially all the slow* ions leaving the plasma and reaching the detector. The value measured in this way is assumed to pertain to the central plasma region, where the density is expected to be highest. A secondary-electron-emission type of fast-atom detector also monitors the density, and tracks reasonably well the values determined by the other detectors. Values of B at the center of the BBII magnetic well (usually 10.3 kG) are obtained from the superconducting-coil current, and W_i is taken as the mean plasma energy, estimated either from the measured energy spectrum of charge-exchange neutrals leaving the plasma region or from the neutral-beam composition. For most of the BBII thresholds, H^+ is the plasma ion.

In Fig. 2 we show selected groups of threshold points plotted in the same way as in Fig. 1, and all obtained at the same value of central magnetic field. Each group is distinguished by the variation of a particular experimental parameter. To obtain the sets denoted by the squares and circles, with W_i values of 1.3 and 0.8 keV, respectively, a metal limiter was gradually moved toward the center of the plasma, in the plane of the field-line fan, at an angle of about 30 deg with the magnetic axis. Because of azimuthal precession and axial reflection, particles that reflect at a value of B greater than that at the inner tip of the limiter should eventually hit it. Thus, the spatial extent of the plasma should be reduced as the limiter is moved in. Experimentally, we found that the instability threshold dropped rapidly,

---

* Produced from the background gas by charge-exchange and ionization processes.

even though $e\phi$ decreased slowly, as the limiter was moved inward from a position completely outside the plasma to a position about 18 cm from the center (the mirror points are at about 44 cm on axis). The mean plasma energy is assumed not to have changed significantly.

The other sets of threshold points in Fig. 2 show a similarly strong threshold variation, even though quite different experimental parameters were changed. To obtain the points denoted by the crosses ($W_i \approx 1.9$ keV), we varied the area of transmission of the neutral beam at a location after the N_2 neutralizer but before the Ne screen and the sweep tank. The area was changed so that the over-all beam size was not varied significantly; i.e., an adjustable "Venetian blind" collimator was used. The threshold decreased rapidly, as shown by the data, as the open area of the collimator was varied from 100% (wide open) to 12.5%. For the remaining two sets of threshold points in Fig. 2, the background-gas conditions in the plasma region were varied. To obtain the threshold points denoted by the triangles ($W_i \approx 0.8$ keV), we admitted N_2 gas into the confinement region through a port below the plasma. As the flow of gas was increased, the plasma decay time decreased from about 1400 to around 200 ms, and the threshold level dropped as shown. The diamond points ($W_i \approx 1.9$ keV) were obtained by varying the density of the Ne screen in the beam line before the main chamber. This affected the amounts of both Ne and N_2 streaming through the plasma region from the beam line. To obtain the threshold drop shown, the Ne flow rate to the screen was decreased by a factor of about 2.5. (At $W_i \approx 0.8$ keV, little change in threshold was observed as the Ne flow rate was dropped.)

The instability-threshold data as plotted in Figs. 1 and 2 do not agree with the BBI results and have a large spread. On an ε vs $e\phi/W_i$ plot, the threshold trend for each of the various individual sets of measurements shown, where diverse experimental parameters were varied, is much steeper than the BBI trend. Also, in comparison with the BBI results, the threshold values in Figs. 1 and 2 tend to fall low. The spread of the data points is well outside the estimated experimental uncertainty, as indicated by the typical error bar on one point in Fig. 1.

Some order can be made out of the spread of threshold points in Fig. 1 by grouping the data according to mean energy. This has been done in Fig. 3, where the data of Fig. 1 are shown again, but this time with different symbols denoting different energy ranges. Lines showing average trends of two of the energy groups have been added. One might imagine, discounting the scatter, that each energy group defines a steep trend like that in Fig. 2. The lower the energy of the group, the further the group is shifted to higher values of $e\phi/W_i$. This spread in the threshold data and the general lack of correlation with our previous work indicate that $e\phi/W_i$ is no longer the controlling parameter for the onset of the instability.

The impression now conveyed by the BBII threshold data is different from the picture given earlier[2,3] when only about 10% of the present number of measurements existed. That initial threshold data approximately followed the BBI 45-deg line to $e\phi/W_i \approx 0.1$, and then deviated from it, forming a plateau region. Many of those earlier threshold points that lay close to the BBI line have now been displaced to the right because of better estimates of mean plasma energy: some of the former values of mean energy have been revised downward considerably because of the large half-energy component found in the beam. The plateau originally observed was formed because, as the neutral beam energy was lowered, a region was reached where ε and ϕ at threshold stopped increasing, and thereafter changed little as the energy was lowered further. When these almost-constant threshold results were displayed on an ε vs $e\phi/W_i$ plot, the decreasing W_i spread them out horizontally, thus forming a plateau. As further threshold data were accumulated, under various vacuum conditions, the plateau effect continued to be seen but at different ε levels at different times. Supposedly, the level of the plateau was dependent on the vacuum conditions. When many threshold measurements, taken under various conditions, are combined as in Fig. 3, the plateau effect no longer is particularly apparent. Instead, one notes the steep variation at each energy that was discussed above, with the different energy groups being displaced with respect to one another.

In an attempt to obtain an improved correlation of the threshold data, we have tried plots of simply n_i versus $e\phi$. For example, in Fig. 4 we have replotted the thresholds for the individual runs of Fig. 2. A fairly well-defined band is formed showing a strong variation of n_i with $e\phi$. The straight line is an approximate fit. A similar plot in Fig. 5 displays all the published BBI data and a general sample of the BBII results. The totality of these threshold points, obtained over a period of about $5\frac{1}{2}$ years, shows a strong and reasonably well-defined variation of n_i with $e\phi$. Density values range over a factor of almost 600. The BBI results tend to be in the lower density region, and the BBII results in the higher, with overlapping of the two groups in the central region. The general correlation observed between the two experiments tends to reassure us that our experimental measurements are not greatly in error.

A summary of the BBII and BBI threshold data is given in Table I. Except for the few additions on the right, all entries in the table were reproduced from punched cards that were prepared for use in the data-analysis program REDUCE.*

III. Corroboration by Classical Collisional Equations

The fairly good correlation observed in the data and the steep variation obtained, when density is plotted against plasma potential (or $e\phi$), are apparently manifestations of the classical collisional equations. Even though the densities are threshold densities and thus pertain to the plasma instability, as a group they still must satisfy the classical relations because the plasma is essentially stable.

A way to write the classical equations, convenient for our present analysis, is

$$e\phi = \left(\frac{(1.8 \times 10^{-12})\, n_i W_i}{n_o \left(\overline{\sigma_i^{\,i} v} + \overline{\sigma_i^{\,e} v_e} + \overline{\sigma_{cx} v} \right) + n_i \overline{\sigma_s^{\,i} v}} \right)^{\frac{2}{5}} \left(-\ln K \right)^{\frac{3}{5}} \qquad (1)$$

*This program was developed by Neil Maron (report in preparation) upon the suggestion of Brendan McNamara, with our data-analysis needs particularly in mind. It has been very useful in our analysis of the large amount of available threshold data (see Secs. III and IV).

and

$$kT_e = \frac{e\phi}{-\ln K} \quad , \tag{2}$$

where

$$K = \frac{n_o(\sigma_i^i V + \overline{\sigma_i^e V_e} + \sigma_{cx} V)}{n_i(\overline{\sigma_s^e V_e})} + \frac{\overline{\sigma_s^i V}}{\overline{\sigma_s^e V_e}} \; . \tag{3}$$

These equations are obtained from Eqs. (12) through (14) of Ref. 4. For the derivation of these equations and for definition of the quantities involved, refer to that article. We use the relations

$$\overline{\sigma_s^e V_e} = (1.4 \times 10^{-7})(0.04/e\phi)^{3/2} \tag{4}$$

and

$$\overline{\sigma_s^i V} = (2 \times 10^{-10}) \; W_i^{-3/2} \; . \tag{5}$$

In Eq. (4)[5] we have used an electron temperature equal to $e\phi$, saying that the electrons of interest here are those with energy about equal to the plasma potential (i.e., they are electrons that can just escape). Equation (5) is a rearrangement of[6]

$$n_i \tau_s \; [=1/\overline{\sigma_s^i V}] \; \approx \; (5 \times 10^9) \; W_i^{3/2} \; .$$

In Eqs. (1) through (5), the quantities W, $e\phi$, and kT_e are in keV.

We also use the equation

$$n_o(\sigma_i^i V + \overline{\sigma_i^e V_e} + \sigma_{cx} V) = \beta C_1 / n_i \quad , \tag{6}$$

where β is the slow-ion current to an end-loss detector, C_1 is the appropriate calibration factor, and the left side is summed over all the gas species in the plasma region. The ionization and charge-exchange processes represented by the three σv terms in Eq. (6) produce the slow ions, which are then accelerated by the plasma potential along field lines out the mirrors. The product βC_1 is divided by n_i because the slow-ion current is proportional to the trapped-fast-ion density as well as to the background-gas density. We have tried using slow-ion currents to two different detectors in the present analysis: Low-Energy Ion Spectrometer (LEIS)[7] and a gridded detector near the magnetic axis at the north end of the magnetic field (GD)[8]. Because LEIS is more sensitive to alignment than GD, we use the GD results in the detailed analysis to follow, for possibly more consistent results.

To show that these equations suggest a strong variation of n_i with $e\phi$, as evidenced by Figs. 4 and 5, we rewrite Eqs. (1) and (3) as follows:

$$\left(\frac{n_i W_i}{n_o \sum \sigma v}\right)\left(-\ln K\right)^{3/2} \propto \left(e\phi\right)^{5/2} , \qquad (7)$$

where

$$K = \frac{n_o \sum \sigma v}{n_i \left(\overline{\sigma_s^e v_e}\right)} \qquad (8)$$

and

$$\sum \sigma v = \sigma_i^i v + \overline{\sigma_i^e v_e} + \sigma_{cx} v \quad . \qquad (9)$$

For simplicity, the ion-scattering terms have been dropped here. For much of our threshold data, these terms are relatively small. Disregarding all the factors on the left of the proportionality sign in Eq. (7) except for the first n_i, one notes a $n_i \propto (e\phi)^{5/2}$ relation. The other factors tend to increase the variation of n_i with $e\phi$. In particular, the dependence on $e\phi$ of the electron-ionization term $\overline{\sigma_i^e v_e}$ and of the electron-scattering term $\overline{\sigma_s^e v_e}$ strengthen the variation. Hence, the strong relationship between n_i and $e\phi$ displayed in Figs. 4 and 5 is not surprising. [Variations in other variables in Eqs. (7) through (9), such as n_0 and W_i, will tend to blur the $n_i - e\phi$ relation somewhat.]

The classical equations have been used to check in some detail the accuracy of our experimental measurements for two of the sets of data in Fig. 4 (circles and crosses). For this analysis we rewrite Eqs. (1) and (3) once again, this time using Eqs. (4) through (6):

$$\left(\frac{(1.8\times10^{-12})\,W_i}{\dfrac{\beta C_1}{n_i^2}+(2.0\times10^{-10})\,W_i^{-3/2}}\right)(-\ln K)^{3/2}=(e\phi)^{5/2}, \quad (10)$$

where

$$K=\frac{\beta C_1}{n_i^2(1.4\times10^{-7})(0.04/e\phi)^{3/2}+(1.4\times10^{-3})(e\phi/0.04W_i)^{3/2}}. \quad (11)$$

For each of the threshold determinations in the two sets of data considered, we substituted into the left-hand side of Eq. (10) and into Eq. (11) the experimental values of n_i, W_i, ϕ, and β, calculated ϕ from Eq. (10), and compared it with the measured ϕ. Expecting that the measured values of n_i might have the largest uncertainty of any of the experimental quantities, and anticipating a possible systematic correction (to be discussed later), we allowed the n_i values in each set to be corrected according to $(90/\phi)^{C_2}$. The quantity C_2 is an adjustable constant, and the number 90 was chosen to minimize the correction in the region where we have the greatest concentration of threshold measurements.

Agreement between the classical equations and experimental results means that each ϕ calculated from Eqs. (10) and (11) should be about equal to its corresponding experimental value. Our procedure here is to find values of C_1 and C_2 that give this agreement, and then, from other considerations, to determine if these numbers are reasonable ones. Figures 6 and 7 show the intermediate results of this analysis. There we have plotted the calculated versus the experimental value of $(\phi/100)^{2.5}$ for each of the individual thresholds considered. We have chosen three values of C_1, spread over a factor of ten in magnitude and corresponding to n_i in units of 10^9 cm^{-3} in Eqs. (10) and (11). For each C_1 and for each of the two sets of data analyzed, we have varied C_2 to give a 45-deg line on these plots. For agreement between theory and experiment, the plotted points should fall on the $\phi_{calc.} = \phi_{exper.}$ 45-deg line in each figure. Therefore, from the results in Figs. 6 and 7 we have interpolated to obtain values of C_1 and C_2 that will give this agreement: $C_1 = 1.23 \times 10^{-10}$ and $C_2 = 0.41$ in Fig. 6, and $C_1 = 5.7 \times 10^{-11}$ and $C_2 = 0.50$ in Fig. 7.

Our best experimental estimate of the calibration factor C_1 is $(2 \pm 1) \times 10^{-10}$, for n_i in units of 10^9 cm^{-3}, when using GD measurements of β. This value of C_1 is obtained from the corresponding LEIS calibration factor* as calculated from detailed observations with LEIS of the relative amounts of the different gas components in the plasma region. By comparing total slow-ion

*Supplied by Ronald K. Goodman.

currents measured by GD and LEIS, we then convert to a value of C_1 for the GD data.

When comparing the experimental estimate of C_1 with the interpolated values that give the desired $\phi_{calc.} = \phi_{exper.}$ lines in Figs. 6 and 7, an approximation made in obtaining Eq. (14) of Ref. 4 [our Eq. (3)] should be first improved upon. There, the quantity $F(e\phi/kT_e)$, which is the fraction of scattered electrons having sufficient energy to escape over the potential barrier, is approximated by $\exp(-e\phi/kT_e)$. For $e\phi/kT_e$ in the range 1.5 to 3.0, which includes the data presently being considered, the calculated ratio $F(e\phi/kT_e)/\exp(-e\phi/kT_e)$ varies from 1.76 to 2.29. If we pick 2.0 for a representative value of this ratio, then, to account for this correction, a factor of 2.0 is added to the denominator of the two terms in Eq. (11). When this correction is included in the analysis leading to Figs. 6 and 7, the values of C_1 must be raised by about 28% to give results like those plotted in these figures. Thus, the interpolated values of C_1 to give the desired $\phi_{calc.} = \phi_{exper.}$ lines in Figs. 6 and 7 become about 1.6 and 0.7 x 10^{-10}, respectively, to be compared with the experimental estimate of $(2 \pm 1) \times 10^{-10}$.

This good agreement between the experimental estimate of C_1 and the values needed in the classical equations so that $\phi_{calc.} \approx \phi_{exper.}$ suggests that the measured quantities describing the experimental thresholds are reasonably accurate. In particular, if we assume that the experimental values of W_i, ϕ, and β are substantially correct, we have a check on the validity of the n_i values. The quantities C_1 and n_i enter into Eqs. (10) and (11) only as the ratio C_1/n_i^2. Thus, a factor-of-2 change in C_1 means a change in n_i of only $\sqrt{2}$ in order not to change C_1/n_i^2 and thus not upset the

$\phi_{calc.} = \phi_{exper.}$ agreement between the classical equations and the two sets of data analyzed here. It appears that no more than this amount of uncertainty in density is warranted, on the basis of the satisfactory comparison between the required and experimentally estimated values of C_1 given just above. (We actually used the average-density values of Table I in the foregoing analysis instead of the peak densities. These latter may be ≈50% greater and are assumed to correspond to the measured values of ϕ. However, this correction to peak density is comparable to the relatively small uncertainty just discussed, and thus is not of major consequence.)

Not only is little change in magnitude of the two sets of experimental density values needed for agreement with the classical equations, but also little change is necessary in the n_i vs ϕ slope of either of the data sets. This is shown by the small values of C_2 required to obtain the 45-deg slopes in Figs. 6 and 7 for over a factor of 10 in C_1. It appears that, at most, a correction roughly proportional to $(1/\phi)^{\frac{1}{2}}$ is needed, which is a relatively small change in the original n_i vs $e\phi$ slope of about 3.5. Thus, the measured slope for n_i vs ϕ is within 14% of that predicted theoretically.

This indicated systematic correction is qualitatively consistent with what one would expect. In the preceding analysis, we effectively assumed a constant factor for conversion from the measured average density to the peak density at the center. As n_i and ϕ increase, the ratio of peak to average density is expected to decrease because of additional ion scattering and spatial spreading. These effects will tend to give a variable conversion factor and a decreased slope for peak density vs ϕ, as suggested by the numerical analysis above.

The classical collisional equations thus have helped check the accuracy of our threshold-density measurements. In effect, we have used the classical equations, which turn out to be quite sensitive to the density values when used in the form of Eqs. (10) and (11), to confirm the experimental density calibration. Unless there is some strong density peaking effect that varies sharply with potential but does not greatly affect the measured values of potential, it appears that our measurements of the magnitude of n_i at threshold and the variation of n_i with ϕ are reasonably accurate.

We assume that the two sets of data analyzed in detail here are representative of all the BBII threshold data in this report. The reasonable agreement obtained between the values of the four measured parameters and the classical predictions gives us more confidence in the threshold measurements and their apparent variance with the BBI theory.

IV. Comparison with Baseball I Theory

The BBI instability-threshold theory, which is based on Landau damping of electron plasma waves, is represented by the equation[1]

$$\varepsilon \equiv (\omega_{pi}/\omega_{ci})^2 = (k_\perp a_i)^2 (e\phi/W_i) \quad . \tag{12}$$

According to this theory, the plasma should be unstable when the parameters for the maximum-density portion of the plasma define a point above the region delineated by Eq. (12) on an ε vs $e\phi/W_i$ plot; and the plasma should be quiescent when the point is below. In reality, the BBI data are considerably spread about an average 45-deg line on the ε vs $e\phi/W_i$ log-log plot. The plausible interpretation that was suggested for this scatter in the data is that of a normal-mode structure for $k_\perp$:

$$k_{\perp m} = (k_r^2 + k_\theta^2)^{1/2} = [(0.25)^2 + (m/6.9)^2]^{1/2} \text{ cm}^{-1}. \qquad (13)$$

When the quantity m takes on the appropriate integral value from 1 through 6 for each threshold determination, the resulting values of $k_{\perp m}$ agree well, in general, with the experimental $k_\perp$ structure. While the numerical values in Eq. (13) were selected to give this correspondence, the choices are reasonable when compared with BBI plasma dimensions.

The procedure used in the BBI experimentation is as follows: If the plasma density is varied (usually by changing the source arc current and thus varying the beam level), a line of slope 2.5 or greater on an ε vs $e\phi/W_i$ plot is defined. This assumes that B and W_i are constant, so the behavior observed is that of n_i vs $e\phi$ (because $\varepsilon \propto n_i/B^2$). The steep slope is that from the classical relation Eq. (1). In one region along this line of steep slope, where the line intersects the 45-deg threshold line defined by Eq. (12), the plasma passes from the stable to the unstable regime (as the beam level increases). If we then change the experimental conditions (the vacuum, for example) and again vary the beam level, a new line of steep slope is defined, displaced from the first. If the vacuum conditions are poorer, it is displaced to the left. One threshold point is found along this line, again where it crosses the line defined by Eq. (12). By varying the plasma conditions, a series of thresholds can be determined. The array of these thresholds will then give the 45-deg-line behavior of Eq. (12), neglecting the complication introduced by the possible spread in $k_\perp$ mode number. (On the n_i - $e\phi$ plot of Fig. 5, such an array tends to disperse the data but does not destroy the over-all classical steep-slope trend.)

The situation in BBII seems to be different. We have seen that varying a particular parameter gives an array of threshold points with a slope much steeper than a 45-deg line. For example, refer to the set of seven triangle points in Fig.2, where vacuum conditions were varied as discussed above for BBI. The slope for this set is definitely steeper than that of the BBI average-threshold line. The BBII results just do not seem to fit the earlier theory.

One question to consider when trying to relate the BBII data to the BBI Landau-damping theory is whether the steep threshold variation observed could be a result of continuous $k_\perp$-mode switching. Figure 8 gives the histogram showing the distribution of values of $\ln k_\perp$ for the BBII data of Table I. A similar type of plot was previously obtained for BBI.[1] We use Eq. (12) to calculate $k_\perp$ for each threshold determination, substituting in experimental numbers for the other parameters. As a guide, some mode assignments are given above the distribution. Mode numbers for the BBI fit are shown, plus two further, somewhat arbitrary, fits. Unlike the BBI results, nothing strongly suggestive is evident. If quantization does occur, the high mode numbers apparently needed give levels so close together that it is difficult to distinguish them in our data. The large peak at $\ln k_\perp \approx 0.8$ should be discounted -- it is at the level where we made many of the periodic threshold checks. Although $k_\perp$ quantization is not distinct in the BBII threshold data, it cannot be ruled out entirely.

Quantities involved in the theory of Eq. (12) include the gyroradius a_i and the parallel wave number $k_\parallel$ as well as the perpendicular wave number $k_\perp$. Figure 9 shows a plot of $k_\perp$ vs a_i and includes both the

BBI and BBII sets of threshold data of Table I. A plot of $k_{\parallel}$ vs $k_{\perp}$, again for all the data, is given in Fig. 10. To obtain $k_{\parallel}$ one can use

$$k_{\parallel} = \frac{k_{\perp}}{\left(\frac{m_i}{m_e}\right)^{\frac{1}{2}} \varepsilon^{\frac{1}{2}}} = \frac{1}{\left(\frac{m_i}{m_e}\right)^{\frac{1}{2}} a_i \left(\frac{e\phi}{W_i}\right)^{\frac{1}{2}}} , \qquad (14)$$

where m_i/m_e is the ion-electron mass ratio. Equation (14) is derived from the equations in Ref. 1 for the fundamental mode (n=1). The plots in Figs. 9 and 10 were made directly with the aforementioned data-analysis program REDUCE. The straight lines shown are first-order, log-log, least-squares fits automatically made by the program. These plots show the different ranges of these pertinent parameters in the two experiments, using the equations of the BBI theory.

We should mention that the variable W_i in Eq. (12) is really the perpendicular component of the plasma-ion energy. In its place we have used the full mean energy throughout this report. The error in doing this should not, in general, be large because most of the thresholds were obtained under conditions where ion-ion scattering was not significant. For the threshold points with the highest values of ε and $e\phi/W_i$ (upper-right points in Fig. 1), where considerable ion-ion scattering occurred, reducing the full mean energy to its perpendicular component would noticeably increase $e\phi/W_i$ and these points would be moved to the right. However, they would be moved by less than a factor of 1.3 (estimated for a scattered distribution in a magnetic well with depth of 2:1).

V. Concluding Remarks

There is no satisfactory explanation for our threshold data at this time. As one searches for an interpretation, there are differences in the BBI and

BBII experiments that should be kept in mind. For example, the neutral beam in BBII passes through the central region at an angle of 90 deg with respect to the magnetic axis instead of at the 61-deg angle in BBI. This geometric difference, along with the plasma-trapping mode of plasma formation in BBII instead of Lorentz trapping only, accentuates the density peak at the minimum of the well. (However, the Phoenix II experiment used perpendicular injection, had a small amount of plasma trapping, and still gave results that seemed to fit the BBI instability theory.[9]) In BBI the vacuum-chamber wall intersected the magnetic axis somewhat inside the maximum-field region, while in BBII the chamber wall is outside the mirror region. Another difference between BBI and BBII is that densities in the latter are in general considerably higher, as shown in Fig. 5. Also, the gyroradii are smaller in BBII, both absolutely and relative to the plasma dimensions. In addition, points in Fig. 1 plotted at the extreme top and right represent plasma conditions for which there was considerable ion-ion scattering. None of the thresholds of BBI was obtained under these conditions.

It was earlier thought that the radial boundary conditions might be affecting the threshold. So, between the final two running periods in which we investigated vacuum-buildup plasma formation, we moved outward or removed entirely probes near the midplane around the circumference of the plasma. These changes had little or no effect either on the maximum-obtainable threshold level or on the steep variation of the threshold on an ε vs $e\phi/W_i$ plot. (However, applying +300 V to a large isolated screen, which was outside the plasma in the midplane at 24 cm from the center of the plasma, appeared to lower the threshold level considerably.)

The role of the plasma potential in the BBII instability is unclear. It appears that, from the threshold data, we cannot say which of two extremes is true. On the one hand, the potential does not seem to affect the threshold; that is, the threshold is dependent on one or more other quantities. According to this point of view, as the threshold density changes, being affected by an unknown parameter, the potential adjusts according to the classical theory. We therefore obtain the classical relation between density and potential. On the other hand, it might be that the threshold is strongly dependent on the potential. In Sec. IV, we discussed how, according to the BBI theory, when a parameter such as the background gas is varied, a series of threshold points is obtained delineating a 45-deg line on an ε vs $\epsilon\phi/W_i$ or n_i vs $e\phi$ log-log plot. Using the same reasoning, one can imagine what would happen if an instability should give a variation of threshold density with potential much steeper than 45 deg. If a parameter such as the background gas were then varied, a set of threshold points would again be obtained at the intersections of the various classical n_i - $e\phi$ lines and the threshold region. This time the set of threshold points would define the steep variation pertinent to this instability. It appears that, if this latter case is true, the dependence of the threshold on ϕ is close to that of the classical behavior. The uncertainties in our threshold data make it difficult to differentiate between the two possibilities just discussed.

With $e\phi/W_i$ apparently no longer the controlling parameter for the instability, and with the role of the plasma potential unclear, the question is raised as to what is important. One wonders what is the common denominator affecting the threshold in the experimentation leading to the data in Fig. 2, for which such dissimilar experimental variables were changed. The purity of the injected neutral beam is not clearly a parameter pertinent to the threshold level. Whether the incident-beam composition is predominantly full energy, predominantly half energy, or a roughly equal mixture, the thresholds still fall considerably below the BBI line, and the steep variation with $e\phi$ is still evident.

One parameter that does seem to be still pertinent is ε, which is proportional to $n_i M/B^2$. As B is increased, both the threshold and maximum (instability-limited) densities increase approximately as B^2. Also, in one series of measurements (data are not included in Table I), where we changed from pure H_2 gas in the source to pure D_2, the threshold density dropped to 0.54 of its value with pure H_2. This drop counteracted the change in M of a factor of 2, and thus ε was held almost constant.

The threshold density may also depend on the spatial distribution of the injected neutral beam. There are some threshold measurements (all the data not included in Table I) that suggest that, when the beam is restricted by a collimating aperture, the threshold density decreases while the corresponding value of $e\phi/W_i$ increases. This is in contrast to behavior such as that illustrated in Fig. 2.

Acknowledgments

The experimental data presented in this report exist only because of the endeavors of the entire Baseball II group. There is much unmentioned effort involved in providing experimental apparatus that functions reliably and measurements in which one can have confidence. Those who especially helped to obtain and interpret the instability-threshold measurements discussed here are Archer H. Futch, Ronald K. Goodman, and Gary D. Porter.

References

1. C.C. Damm, J.H. Foote, A.H. Futch, Jr., A.L. Hunt, K. Moses, R.F. Post, and J.B. Taylor, Evidence for Collisionless Damping of Unstable Waves in a Mirror-Confined Plasma, Phys. Rev. Letters 24, 495 (1970).

2. Controlled Thermonuclear Research Annual Report, Lawrence Livermore Laboratory, Rept. UCRL-50002-73 (1973), p. 27.

3. J.H. Foote, C.C. Damm, A.H. Futch, R.K. Goodman, F.J. Gordon, G.W. Hamilton, A.L. Hunt, J.E. Osher, and G.D. Porter, Instability Density Limitation in Baseball II, Bull. Am. Phys. Soc. 18, 1318 (1973).

4. A.H. Futch, C.C. Damm, J.H. Foote, A.L. Gardner, and J. Killeen, Collisional Processes at Low Densities in Magnetic Mirror Systems, Phys. Fluids 14, 1542 (1971).

5. Equation (4) can be obtained, for example, from Eqs. (41) and (43) of R.F. Post, Controlled Fusion Research - An Application of the Physics of High Temperature Plasmas, Rev. Mod. Phys. 28, 338 (1956). The numerical coefficient has been changed slightly to that used on p. 1287 of A.H. Futch, Jr., W. Heckrotte, C.C. Damm, J. Killeen, and L.E. Mish, Plasma Production by Neutral-Atom Injection: Equations and Numerical Solutions, Phys. Fluids 5, 1277 (1962) [UCRL-6728].

6. O.A. Anderson, D.H. Birdsall, C.C. Damm, J.H. Foote, A.H. Futch, R.K. Goodman, F.J. Gordon, G.W. Hamilton, E.B. Hooper, A.L. Hunt, J.E. Osher, and G.D. Porter, Plasma Production and Confinement in the Baseball II Mirror Experiment, UCRL-75512 Preprint, IAEA Fifth Conference on Plasma Physics and Controlled Nuclear Fusion Research, Tokyo, Japan, November 11-15, 1974, Table I.

7. Ronald K. Goodman, Mass Analysis of Low-Energy Ions in the Baseball II Plasma Containment Experiment, UCRL-74165 Preprint (July 1974).

8. Controlled Thermonuclear Research Annual Report, Lawrence Livermore Laboratory, Rept. UCRL-50002-73 (1973), p. 30.

9. E. Thompson. J.G. Cordey, and D.R. Sweetman, Experimental and Theoretical Investigation of Plasma Build-up and Microinstabilities in a Neutral-Injection Mirror Machine, Proceedings of the Fourth International Conference on Plasma Physics and Controlled Nuclear Fusion Research, Madison, Wisconsin, Vol. II, p. 689 (1971).

TABLE I

SUMMARY OF THE BASEBALL II AND BASEBALL I INSTABILITY-THRESHOLD DATA.

REFER TO THE NOTES AT THE END OF THIS TABLE.

ORDER OF THRESHOLD EXPERIMENTAL PARAMETERS ON DATA CARDS:

SET#	CARD#	DATA SET	DENSITY	EPSILON	POTENTIAL	ENERGY	MAGN FLD	DECAYTIME
SET#	CARD#	MASS	BEAM CUR.	COLLIMATR	LEIS BETA	GD BETA		

BASEBALL II

1	1	1.	0.95	0.205	155.	1.34	10.3	1090.
1	2	1.	0.	0.	0.			
2	1	2.	1.05	0.227	138.	0.83	10.3	2040.
2	2	1.	0.	0.	0.			
3	1	3.	1.02	0.220	130.	0.43	10.3	1470.
3	2	1.	0.	0.	0.			
4	1	4.	1.42	0.226	134.	0.43	12.0	1000.
4	2	1.	0.	0.	0.			
5	1	5.	1.14	0.182	157.	1.34	12.0	1140.
5	2	1.	0.	0.	0.			
6	1	6.	1.25	0.199	148.	0.83	12.0	1190.
6	2	1.	0.	0.	0.			
7	1	7.	0.62	0.193	136.	1.34	8.6	1470.
7	2	1.	0.	0.	0.			
8	1	8.	0.62	0.193	115.	0.43	8.6	1260.
8	2	1.	0.	0.	0.			
9	1	9.	0.53	0.165	127.	0.83	8.6	1650.
9	2	1.	0.	0.	0.			
10	1	10.	0.91	0.197	145.	1.34	10.3	1410.
10	2	1.	0.	0.	0.			
11	1	11.	0.55	0.119	105.	1.34	10.3	400.
11	2	1.	0.	0.	0.			
12	1	12.	0.28	0.061	93.	1.85	10.3	740.
12	2	1.	0.	0.	0.			
13	1	13.	0.26	0.056	102.	1.85	10.3	380.
13	2	1.	0.	0.	0.			
14	1	14.	0.58	0.125	97.	1.34	10.3	1180.
14	2	1.	1.2	0.	0.			
15	1	15.	0.40	0.086	83.	0.83	10.3	1200.
15	2	1.	1.35	0.	0.			
16	1	16.	0.43	0.093	83.	0.50	10.3	1270.
16	2	1.	1.92	0.	0.			
17	1	17.	0.46	0.099	100.	1.34	10.3	1660.
17	2	1.	1.15	0.	0.			
18	1	18.	0.64	0.138	93.	1.34	10.3	1250.
18	2	1.	1.25	0.	0.			
19	1	19.	0.54	0.117	83.	0.83	10.3	1210.
19	2	1.	1.74	0.	0.			
20	1	20.	0.48	0.104	67.	0.83	10.3	680.
20	2	1.	1.12	0.	0.			
21	1	21.	0.45	0.097	85.	0.83	10.3	1000.
21	2	1.	0.76	0.	0.			
22	1	22.	0.40	0.086	88.	0.50	10.3	1020.
22	2	1.	1.2	0.	0.			
23	1	23.	0.66	0.142	77.	1.34	10.3	820.

23	2	1.	1.78	0.	0.			
24	1	24.	0.64	0.138	72.	0.83	10.3	630.
24	2	1.	2.79	0.	0.			
25	1	25.	0.56	0.121	70.	0.50	10.3	830.
25	2	1.	4.27	0.	0.			
26	1	26.	0.50	0.108	51.	0.83	10.3	400.
26	2	1.	4.67	0.	0.			
27	1	27.	0.162	0.035	40.	1.34	10.3	290.
27	2	1.	3.73	0.	0.			
28	1	28.	0.102	0.022	45.	1.85	10.3	380.
28	2	1.	1.75	0.	0.			
29	1	29.	0.34	0.074	60.	1.34	10.3	790.
29	2	1.	1.78	0.	0.			
30	1	30.	0.52	0.113	70.	1.34	10.3	640.
30	2	1.	1.84	0.	0.			
31	1	31.	0.20	0.043	60.	2.32	10.3	1430.
31	2	1.	1.41	0.	0.			
32	1	32.	0.027	0.0059	29.	11.3	10.3	0.
32	2	1.	28.0	0.	0.			
33	1	33.	0.044	0.0094	49.	5.7	10.3	0.
33	2	1.	5.0	0.	0.			
34	1	34.	0.56	0.121	85.	1.34	10.3	0.
34	2	1.	1.7	0.	0.			
35	1	35.	0.091	0.020	68.	2.85	10.3	0.
35	2	1.	0.8	0.	0.			
36	1	36.	0.27	0.058	71.	1.87	10.3	0.
36	2	1.	1.3	0.	0.			
37	1	37.	0.041	0.0089	35.	3.5	10.3	0.
37	2	1.	3.1	0.	0.			
38	1	38.	0.093	0.0201	63.	3.0	10.3	0.
38	2	1.	0.91	0.	0.			
39	1	39.	0.029	0.013	57.	1.34	10.3	0.
39	2	2.	0.35	0.	0.			
40	1	40.	0.034	0.015	66.	1.34	10.3	0.
40	2	2.	0.24	0.	0.			
41	1	41.	0.17	0.037	71.	1.87	10.3	958.
41	2	1.	0.83	1.	56.5	2.69		
42	1	42.	0.09	0.018	74.	1.87	10.3	1500.
42	2	1.	0.66	4.	30.2	1.16		
43	1	43.	0.32	0.063	85.	0.83	10.3	1236.
43	2	1.	1.14	4.	68.1	3.46		
44	1	44.	0.38	0.082	76.	0.83	10.3	987.
44	2	1.	1.42	1.	90.1	5.64		
45	1	45.	0.35	0.076	76.	0.61	10.3	978.
45	2	1.	1.53	1.	85.0	5.24		
46	1	46.	0.23	0.044	85.	1.34	10.3	1035.
46	2	1.	1.12	4.	85.9	4.18		
47	1	47.	0.20	0.040	69.	1.34	10.3	844.
47	2	1.	0.79	1.	64.9	3.00		
48	1	48.	0.37	0.080	76.	1.09	10.3	963.
48	2	1.	1.52	1.	118.4	6.40		
49	1	49.	0.34	0.071	85.	1.09	10.3	1171.
49	2	1.	1.43	4.	79.2	4.96		
50	1	50.	0.32	0.069	95.	0.61	10.3	1358.
50	2	1.	1.63	4.	32.3			
51	1	51.	0.36	0.077	80.	1.34	10.3	963.
51	2	1.	1.14	1.	116.1			
52	1	52.	0.26	0.052	86.	1.34	10.3	1200.
52	2	1.	1.14	4.	0.			
53	1	53.	0.16	0.026	78.	1.59	10.3	1044.

53	2	1.	0.90	4.	0.			
54	1	54.	0.52	0.109	87.	1.59	10.3	1179.
54	2	1.	1.45	1.	92.3			
55	1	55.	0.35	0.069	99.	1.59	10.3	1653.
55	2	1.	1.22	4.	48.4			
56	1	56.	0.25	0.050	84.	0.83	10.3	1281.
56	2	1.	2.28	4.	102.7			
57	1	57.	0.25	0.055	87.	0.83	10.3	1257.
57	2	1.	1.13	4.	77.3			
58	1	58.	0.22	0.047	94.	1.59	10.3	1277.
58	2	1.	1.08	4.	93.3			
59	1	59.	0.27	0.054	80.	1.59	10.3	1040.
59	2	1.	1.35	4.	119.6			
60	1	60.	0.26	0.058	78.	1.59	10.3	1014.
60	2	1.	0.78	1.	83.8			
61	1	61.	0.39	0.084	81.	1.34	10.3	995.
61	2	1.	1.01	1.	107.6			
62	1	62.	0.33	0.071	84.	1.59	10.3	1212.
62	2	1.	1.21	1.	0.			
63	1	63.	0.22	0.046	93.	1.34	10.3	1699.
63	2	1.	1.20	4.	0.			
64	1	64.	0.36	0.078	74.	0.50	10.3	500.
64	2	1.	1.81	1.	71.7	3.92		
65	1	65.	0.37	0.080	75.	0.83	10.3	861.
65	2	1.	1.43	1.	92.8	5.20		
66	1	66.	0.34	0.075	73.	1.34	10.3	707.
66	2	1.	1.81	1.	144.8	6.76		
67	1	67.	0.037	0.008	55.	1.87	10.3	500.
67	2	1.	.42	1.	45.1	1.17		
68	1	68.	0.098	0.021	57.	1.59	10.3	397.
68	2	1.	1.55	1.	106.4	2.40		
69	1	69.	0.29	0.063	67.	1.34	10.3	834.
69	2	1.	2.15	1.	160.6	6.64		
70	1	70.	0.076	0.016	50.	1.59	10.3	258.
70	2	1.	1.56	1.	87.5	1.83		
71	1	71.	0.083	0.018	52.	1.59	10.3	430.
71	2	1.	1.31	1.	82.0	2.20		
72	1	72.	0.39	0.085	90.	1.59	10.3	1000.
72	2	1.	1.92	1.	124.7	4.72		
73	1	73.	0.47	0.101	90.	1.59	10.3	1000.
73	2	1.	2.30	1.	124.8	5.70		
74	1	74.	0.21	0.047	77.	1.87	10.3	1151.
74	2	1.	1.36	1.	77.9	2.74		
75	1	75.	0.059	0.013	57.	2.32	10.3	500.
75	2	1.	2.00	1.	34.1	2.25		
76	1	76.	0.40	0.087	84.	1.34	10.3	1053.
76	2	1.	1.58	1.	126.7	4.80		
77	1	77.	0.40	0.086	81.	0.83	10.3	965.
77	2	1.	1.33	1.	106.4	3.76		
78	1	78.	0.33	0.071	80.	0.61	10.3	922.
78	2	1.	1.82	1.	89.7	3.52		
79	1	79.	0.22	0.048	77.	0.83	10.3	992.
79	2	1.	0.75	6.	57.5	2.66		
80	1	80.	0.23	0.050	76.	0.83	10.3	867.
80	2	1.	1.29	6.	66.5	3.16		
81	1	81.	0.36	0.078	92.	0.83	10.3	1502.
81	2	1.	1.19	6.	41.4	3.56		
82	1	82.	0.33	0.071	93.	0.83	10.3	1513.
82	2	1.	1.10	6.	39.8	3.66		
83	1	83.	0.38	0.081	84.	0.83	10.3	1188.

83	2	1.	1.19	1.	43.3	4.00			
84	1	84.	0.42	0.090	84.	0.83	10.3	1251.	
84	2	1.	1.09	7.	46.5	4.44			
85	1	85.	0.44	0.096	91.	1.34	10.3	1247.	
85	2	1.	1.15	7.	0.	6.36			
86	1	86.	0.43	0.093	90.	1.34	10.3	1339.	
86	2	1.	1.04	7.	0.	6.12			
87	1	87.	0.19	0.042	75.	1.87	10.3	1428.	
87	2	1.	0.78	7.	0.	2.10			
88	1	88.	0.079	0.017	64.	2.32	10.3	1100.	
88	2	1.	0.79	7.	24.3	1.27			
89	1	89.	0.11	0.024	67.	2.32	10.3	1010.	
89	2	1.	0.95	7.	0.	1.47			
90	1	90.	0.045	0.0097	57.	2.32	10.3	944.	
90	2	1.	0.77	7.	16.9	0.65			
91	1	91.	0.17	0.037	78.	2.32	10.3	1105.	
91	2	1.	1.18	1.	53.9	1.85			
92	1	92.	0.34	0.075	85.	2.32	10.3	1392.	
92	2	1.	1.26	1.	121.6	3.35			
93	1	93.	0.18	0.039	77.	2.32	10.3	1695.	
93	2	1.	0.82	7.	87.3	2.56			
94	1	94.	0.24	0.053	79.	2.32	10.3	1176.	
94	2	1.	1.20	1.	142.9	3.15			
95	1	95.	0.14	0.032	69.	2.32	10.3	1000.	
95	2	1.	0.96	1.	112.2	2.68			
96	1	96.	0.37	0.081	78.	0.83	10.3	1116.	
96	2	1.	1.12	1.	174.2	4.16			
97	1	97.	0.41	0.089	78.	0.83	10.3	1100.	
97	2	1.	1.11	1.	138.5	4.86			
98	1	98.	0.24	0.053	83.	0.80	10.3	1600.	
98	2	1.	2.8	0.	0.				
99	1	99.	0.33	0.072	84.	0.80	10.3	1600.	
99	2	1.	4.1	0.	0.				
100	1	100.	0.016	0.0035	48.	1.9	10.3	0.	
100	2	1.	3.7	0.	0.				
101	1	101.	0.020	0.0043	55.	1.9	10.3	0.	
101	2	1.	2.7	0.	0.				
102	1	102.	0.31	0.066	81.	0.80	10.3	1900.	
102	2	1.	4.0	0.	0.				
103	1	103.	0.20	0.043	79.	0.80	10.3	1700.	
103	2	1.	2.4	0.	0.				
104	1	104.	0.36	0.078	87.	0.80	10.3	1300.	
104	2	1.	2.1	0.	0.				
105	1	105.	0.39	0.084	87.	0.80	10.3	1300.	
105	2	1.	2.2	0.	0.				
106	1	106.	0.28	0.086	76.	0.80	8.6	1750.	
106	2	1.	1.4	0.	0.				
107	1	107.	0.23	0.072	80.	0.80	8.6	2300.	
107	2	1.	1.2	0.	0.				
108	1	108.	0.16	0.081	63.	0.80	6.9	0.	
108	2	1.	0.7	0.	0.				
109	1	109.	0.15	0.074	63.	0.80	6.9	0.	
109	2	1.	0.6	0.	0.				
110	1	110.	0.019	0.0041	30.	0.80	10.3	217.	N_2
110	2	1.	4.1	0.	0.				
111	1	111.	0.39	0.084	93.	0.80	10.3	1600.	
111	2	1.	2.1	0.	0.				
112	1	112.	0.43	0.092	88.	0.55	10.3	1300.	
112	2	1.	2.2	0.	0.				
113	1	113.	0.39	0.084	83.	0.55	10.3	1250.	

(this measurement and the six marked with "N_2" below are the triangle results plotted in Figs. 2 and 4)

113	2	1.	1.7	0.	0.				
114	1	114.	0.38	0.081	90.	0.80	10.3	1350.	
114	2	1.	1.3	0.	0.				
115	1	115.	0.43	0.092	92.	0.80	10.3	1400.	
115	2	1.	2.0	0.	0.				
116	1	116.	0.34	0.073	77.	0.80	10.3	850.	N_2
116	2	1.	2.8	0.	0.				
117	1	117.	0.29	0.062	77.	0.80	10.3	900.	N_2
117	2	1.	2.3	0.	0.				
118	1	118.	0.39	0.084	99.	1.35	10.3	1600.	
118	2	1.	0.9	0.	0.				
119	1	119.	0.30	0.065	88.	1.35	10.3	1800.	
119	2	1.	0.6	0.	0.				
120	1	120.	0.130	0.028	79.	1.9	10.3	1500.	
120	2	1.	0.8	0.	0.				
121	1	121.	0.39	0.084	91.	0.8	10.3	1500.	
121	2	1.	1.8	0.	0.				
122	1	122.	0.27	0.059	72.	0.8	10.3	800.	
122	2	1.	2.9	0.	0.				
123	1	123.	0.36	0.078	83.	0.8	10.3	1050.	
123	2	1.	2.3	0.	0.				
124	1	124.	0.34	0.073	77.	0.55	10.3	1100.	
124	2	1.	2.0	0.	0.				
125	1	125.	0.41	0.089	91.	0.8	10.3	1400.	N_2
125	2	1.	1.7	0.	0.				
126	1	126.	0.28	0.061	73.	0.8	10.3	900.	
126	2	1.	2.8	0.	0.				
127	1	127.	0.22	0.047	68.	0.8	10.3	900.	N_2
127	2	1.	2.1	0.	0.				
128	1	128.	0.093	0.020	51.	0.9	10.3	600.	N_2
128	2	1.	2.4	0.	0.				
129	1	129.	0.065	0.014	52.	0.9	10.3	600.	N_2
129	2	1.	2.1	0.	0.				
130	1	130.	0.031	0.0068	51.	3.0	10.3	0.	
130	2	1.	2.5	0.	0.				
131	1	131.	0.21	0.046	84.	1.59	10.3	1300.	
131	2	1.	1.5	0.	0.				
132	1	132.	0.079	0.017	67.	1.85	10.3	0.	
132	2	1.	1.3	0.	0.				
133	1	133.	0.24	0.052	81.	1.14	10.3	1250.	
133	2	1.	1.1	0.	0.				
134	1	134.	0.185	0.040	85.	1.59	10.3	1100.	
134	2	1.	1.3	0.	0.				
135	1	135.	0.33	0.071	87.	0.80	10.3	1200.	
135	2	1.	1.0	0.	0.				
136	1	136.	0.33	0.071	83.	0.47	10.3	1300.	
136	2	1.	1.8	0.	0.				
137	1	137.	0.41	0.088	90.	0.80	10.3	1400.	
137	2	1.	1.4	0.	0.				
138	1	138.	0.43	0.093	92.	0.80	10.3	1500.	1225
138	2	1.	1.5	0.	0.				
139	1	139.	0.41	0.089	83.	0.80	10.3	1300.	2100
139	2	1.	1.1	0.	0.				
140	1	140.	0.39	0.084	89.	0.80	10.3	1100.	600
140	2	1.	2.6	0.	0.				
141	1	141.	0.33	0.072	81.	0.80	10.3	1100.	600
141	2	1.	2.0	0.	0.				
142	1	142.	0.139	0.030	75.	1.90	10.3	1400.	1225
142	2	1.	1.2	0.	0.				
143	1	143.	0.148	0.032	76.	1.90	10.3	1600.	2100

Neon flow to screen (cc/min)

143	2	1.	0.9	0.	0.				
144	1	144.	0.26	0.057	86.	1.90	10.3	1400.	2100
144	2	1.	1.5	0.	0.				
145	1	145.	0.035	0.0076	55.	1.90	10.3	500.	800
145	2	1.	2.1	0.	0.				
146	1	146.	0.43	0.093	93.	0.80	10.3	1400.	50
146	2	1.	1.4	0.	0.	5.48			
147	1	147.	0.26	0.056	94.	1.90	10.3	1700.	50
147	2	1.	1.5	0.	0.	4.00			
148	1	148.	0.20	0.043	88.	1.90	10.3	1700.	50
148	2	1.	1.1	0.	0.	3.70			
149	1	149.	0.148	0.032	81.	1.90	10.3	1700.	25
149	2	1.	1.0	0.	0.	2.49			
150	1	150.	0.062	0.0134	66.	1.90	10.3	1400.	12.5
150	2	1.	0.9	0.	0.	0.80			
151	1	151.	0.35	0.076	103.	1.90	10.3	1500.	100
151	2	1.	1.7	0.	0.	6.44			
152	1	152.	0.20	0.043	89.	1.90	10.3	1650.	100
152	2	1.	1.0	0.	0.	3.92			
153	1	153.	0.082	0.018	65.	1.34	10.3	900.	41
153	2	1.	0.57	0.	0.	1.32			
154	1	154.	0.16	0.035	75.	1.34	10.3	1500.	36
154	2	1.	0.82	0.	0.	2.62			
155	1	155.	0.25	0.056	81.	1.34	10.3	1370.	31
155	2	1.	1.25	0.	0.	4.82			
156	1	156.	0.40	0.086	85.	1.34	10.3	1240.	26
156	2	1.	1.27	0.	0.	5.53			
157	1	157.	0.40	0.088	86.	1.34	10.3	1270.	20.7
157	2	1.	1.30	0.	0.	7.59			
158	1	158.	0.42	0.090	87.	1.34	10.3	1260.	0 (out)
158	2	1.	1.50	0.	0.	7.68			
159	1	159.	0.39	0.085	79.	0.83	10.3	1090.	0
159	2	1.	1.91	0.	0.	4.60			
160	1	160.	0.27	0.058	75.	0.83	10.3	1140.	31
160	2	1.	1.32	0.	0.	2.81			
161	1	161.	0.096	0.021	57.	0.83	10.3	1510.	41
161	2	1.	0.81	0.	0.	0.76			
162	1	162.	0.34	0.074	75.	0.83	10.3	1140.	25.8
162	2	1.	2.06	0.	0.	3.80			

Open area of Venetian-blind collimator (%)

Relative position of axial limiter. Distance (in cm) from center of plasma to inner tip of limiter is 59 minus relative-position reading.

BASEBALL I

200	1	200.	.0041	.0031	16.	15.	5.03	240.
200	2	1.	.68	0.	0.			
201	1	201.	.0030	.0020	15.	15.	5.26	300.
201	2	1.	.48	0.	0.			
202	1	202.	.0062	.0043	44.	15.	5.21	2250.
202	2	1.	.18	0.	0.			
203	1	203.	.0090	.0062	54.	15.	5.21	1870.
203	2	1.	.34	0.	0.			
204	1	204.	.0030	.0021	19.	15.	5.17	390.
204	2	1.	.73	0.	0.			
205	1	205.	.053	.034	83.	15.	5.40	1200.
205	2	1.	.91	0.	0.			
206	1	206.	.0123	.012	26.	10.	4.41	80.
206	2	1.	17.8	0.	0.			
207	1	207.	.0385	.030	36.	12.	4.92	500.
207	2	1.	5.1	0.	0.			
208	1	208.	.0254	.027	63.	8.	4.25	1210.
208	2	1.	6.1	0.	0.			

209	1	209.	.0194	.034	45.	5.	3.30	1200.
209	2	1.	12.6	0.	0.			
210	1	210.	.0176	.034	39.	5.	3.14	1050.
210	2	1.	17.6	0.	0.			
211	1	211.	.018	.034	52.	5.	4.08	3100.
211	2	2.	10.0	0.	0.			
212	1	212.	.0112	.029	42.	4.	2.68	1170.
212	2	1.	4.75	0.	0.			
213	1	213.	.012	.034	42.	3.	2.57	2300.
213	2	1.	7.32	0.	0.			
214	1	214.	.0112	.064	26.	2.	1.80	1600.
214	2	1.	5.6	0.	0.			
215	1	215.	.0076	.044	28.	2.	1.80	1400.
215	2	1.	4.05	0.	0.			
216	1	216.	.0205	.108	55.	1.5	1.89	3300.
216	2	1.	4.31	0.	0.			
217	1	217.	.0148	.078	53.	1.5	1.89	3300.
217	2	1.	2.87	0.	0.			
218	1	218.	.0075	.041	30.	2.	1.85	1300.
218	2	1.	7.39	0.	0.			
219	1	219.	.0046	.027	30.	2.	1.84	1000.
219	2	1.	4.05	0.	0.			
220	1	220.	.0047	.026	32.	2.	1.85	2350.
220	2	1.	2.99	0.	0.			
221	1	221.	.0030	.020	27.	1.5	1.66	1800.
221	2	1.	2.54	0.	0.			
222	1	222.	.0025	.028	23.	1.	1.29	2100.
222	2	1.	1.0	0.	0.			
223	1	223.	.0139	.025	42.	5.	3.23	900.
223	2	1.	6.61	0.	0.			
224	1	224.	.0067	.0046	35.	15.	5.25	290.
224	2	1.	1.27	0.	0.			
225	1	225.	.0175	.022	37.	5.	3.90	1000.
225	2	1.	5.2	0.	0.			
226	1	226.	.0183	.018	25.	5.	4.35	700.
226	2	1.	7.56	0.	0.			
227	1	227.	.0458	.041	45.	5.	4.56	2000.
227	2	1.	18.5	0.	0.			
228	1	228.	.0376	.035	60.	5.	4.49	1150.
228	2	1.	21.7	0.	0.			
229	1	229.	.0274	.020	45.	5.	5.12	990.
229	2	1.	8.19	0.	0.			
230	1	230.	.0259	.018	54.	5.	5.27	770.
230	2	1.	5.2	0.	0.			
231	1	231.	.0731	.036	77.	5.	6.20	1200.
231	2	1.	18.9	0.	0.			
232	1	232.	.0197	.028	43.	2.	3.64	1500.
232	2	1.	5.63	0.	0.			
233	1	233.	.0279	.040	53.	2.	3.64	1730.
233	2	1.	7.22	0.	0.			

TABLE I NOTES

General

A zero or blank entry in the table means that the particular value has not been entered on the punched data cards. (It still may be available from the data notebooks or from analog magnetic tape.)

Most well-analyzed BBII threshold measurements have been included in this table.

Density

Units -- 10^9 cm^{-3}.

Typical accuracy -- approximately that indicated by the error bar in Fig. 1 (a range of a factor of 2).

BBII results -- average-density values, using microwave-interferometer calibration, where a constant density is assumed over a 20-cm path along a line through the center at about 70 deg to the magnetic axis. These average-density numbers are the values used in Figs. 4 and 5 and in the numerical analysis of Sec. III, which uses the classical equations.

BBI results -- peak-density values.

Epsilon

$$\varepsilon = \left(\frac{\omega_{pi}}{\omega_{ci}}\right)^2 = \left(4\pi M_{H^+} c^2\right)\left(A\, n_i / B^2\right) = (18.8)\,\frac{A\, n_i\left(10^9\,\mathrm{cm}^{-3}\right)}{\left[B(\mathrm{kG})\right]^2},$$

where A is 1 for H^+ and 2 for D^+.

BBII results -- in calculating the values of ε in the table, the average-density values in the table have been multiplied by 1.21 to convert them to peak-density values. (Actually, the plasma radial profiles suggest that a larger number, more like 1.5, would have been a better conversion factor.) The occasional deviation of an ε value in the table from that calculated by the above equation reflects our uncertainty as to the best n_i value to use.

BBI results -- the densities in the table have already been converted to peak values, so no further correction has been made in converting to values of ε.

Plasma Potential

Units -- volt.

Typical accuracy -- ±10% in the retarding-bias determination.

TABLE I NOTES (continued)

Energy
Units -- keV.
Typical accuracy -- $\pm$15%.
The ion-energy numbers given in the table are mean values.

Magnetic Field
Units -- kG.
Typical accuracy -- $\pm$5%.
The values given correspond to the minimum of the magnetic well.

Decay Time
Units -- ms.
Typical accuracy -- $\pm$25% or better.
BBII results:
Data sets #1-9 -- characteristic decay time shortly after beam turnoff of fast-atom detector (FAD).
Data sets #10-162 -- characteristic decay time of nT_e (see Sec. II) shortly after beam turnoff. To convert to the density decay time, approximately, multiply by the factor of 1.4 (assuming $T_e \propto n^{2/5}$ so $nT_e \propto n^{1.4}$ and assuming $n \propto \exp(-t/\tau)$ where τ is the characteristic decay time of the density).
BBI results -- FAD characteristic decay time corrected to beam-on conditions.

Mass
1 for H^+, 2 for D^+.

Beam Current
Units -- mA.
Typical accuracy -- $\pm$25%. (The BBI results may be less certain.)

Collimator
Code: 1 -- open (about 3.5-in. diam.), 4 -- 1.5-in. diam., 6 -- 3.5 in. diam. with top half blocked off, 7 -- Venetian blind collimator. Collimator position for codes 1-6 is in the beam line before the confinement chamber; position for code 7 is further up the beam line toward the source.

LEIS Beta
See Sec. III for explanation -- not used in the analysis described in this report. The magnetic field was reversed from the normal direction for Data Sets #50-71. Because of alignment sensitivity, the calibration for these values of LEIS β may be somewhat different from that for the other recorded values of LEIS β.

GD Beta
The β values in the table obtained from the gridded detector are signal amplitudes in volts for standard amplifier-gain settings. The values of the calibration factor C_1 in Sec. III are those appropriate for these β measurements and for n_i in units of 10^9 cm^{-3}.

Fig. 1. General sample of instability-threshold measurements in BBII, plotted as $\mathcal{E}$ vs $e\phi/W_i$, compared with the BBI results. Typical experimental uncertainty is shown by error bar on one point.

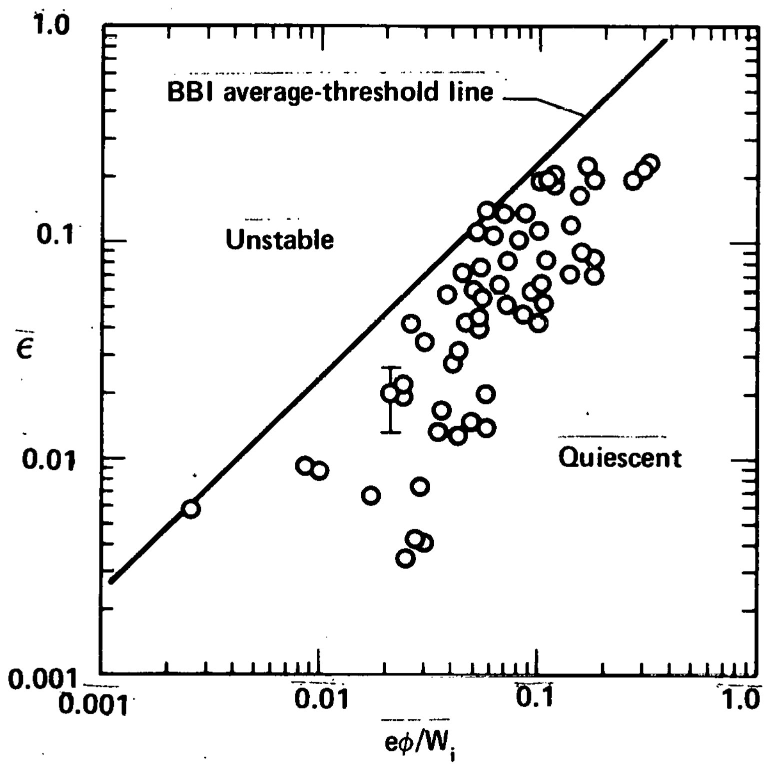

Fig. 2. Selected groups of threshold points, compared with one another and with the BBI results: squares and circles -- axial-limiter position varied, 1.3 and 0.8 keV, respectively; crosses -- area of transmission of neutral beam varied, 1.9 keV; triangles -- N_2 gas in plasma region varied, 0.8 keV; diamonds -- Ne-screen density varied, 1.9 keV.

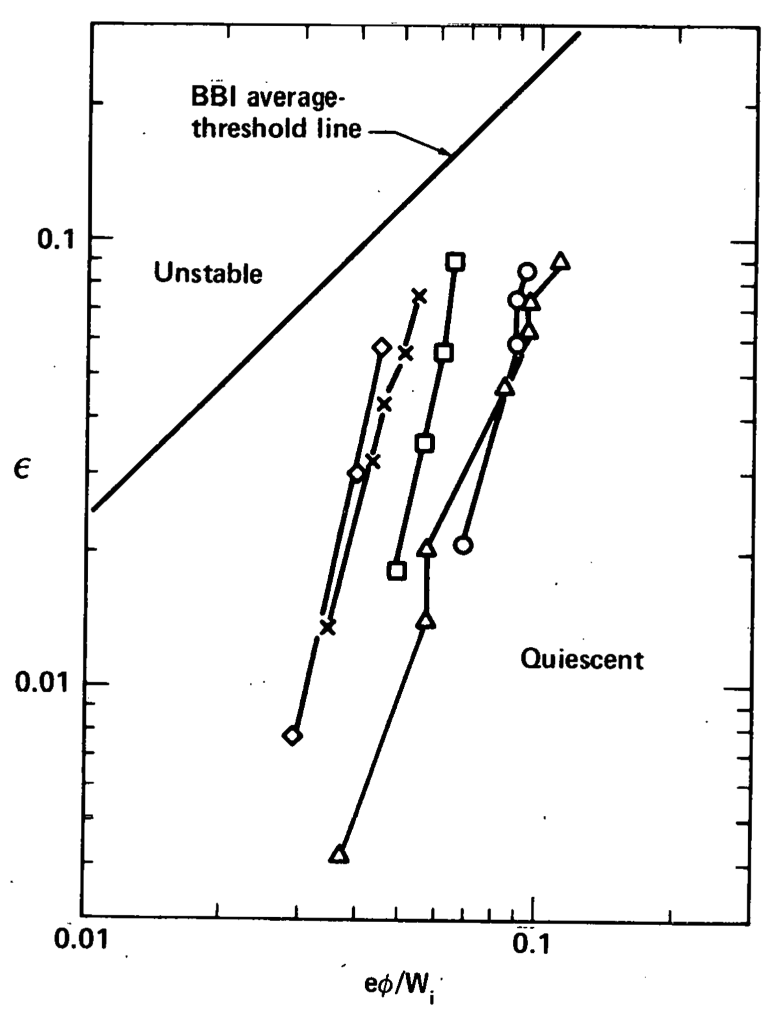

Fig. 3. Threshold data of Fig. 1, plotted again as $\mathcal{E}$ vs $e\phi/W_i$, but now with different symbols denoting different energy ranges. Average trends of two of the energy groups are indicated.

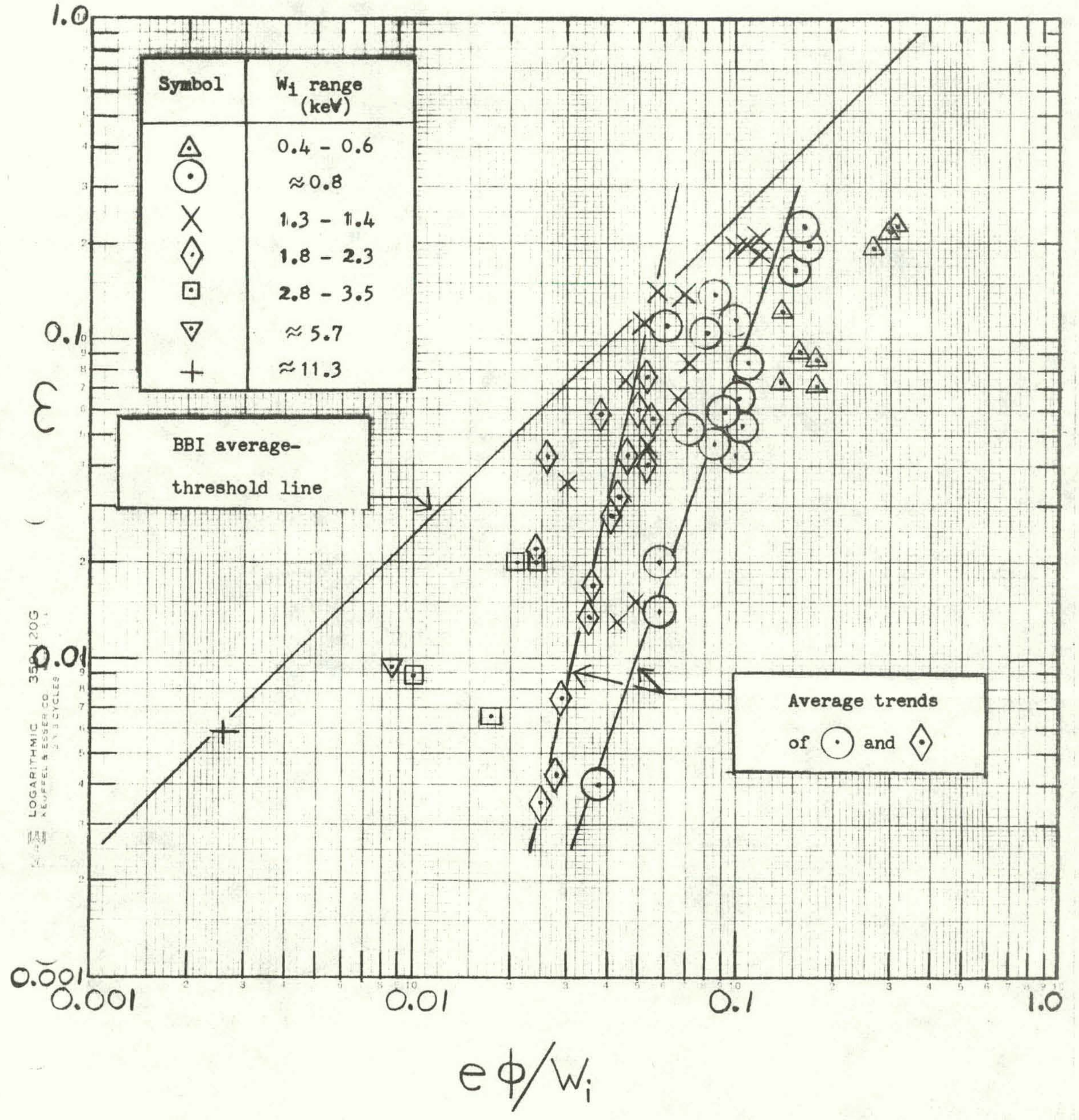

Fig. 4. Same threshold data as in Fig. 2, but now plotted as ion density vs $e\phi$. An approximate fit to the data is shown.

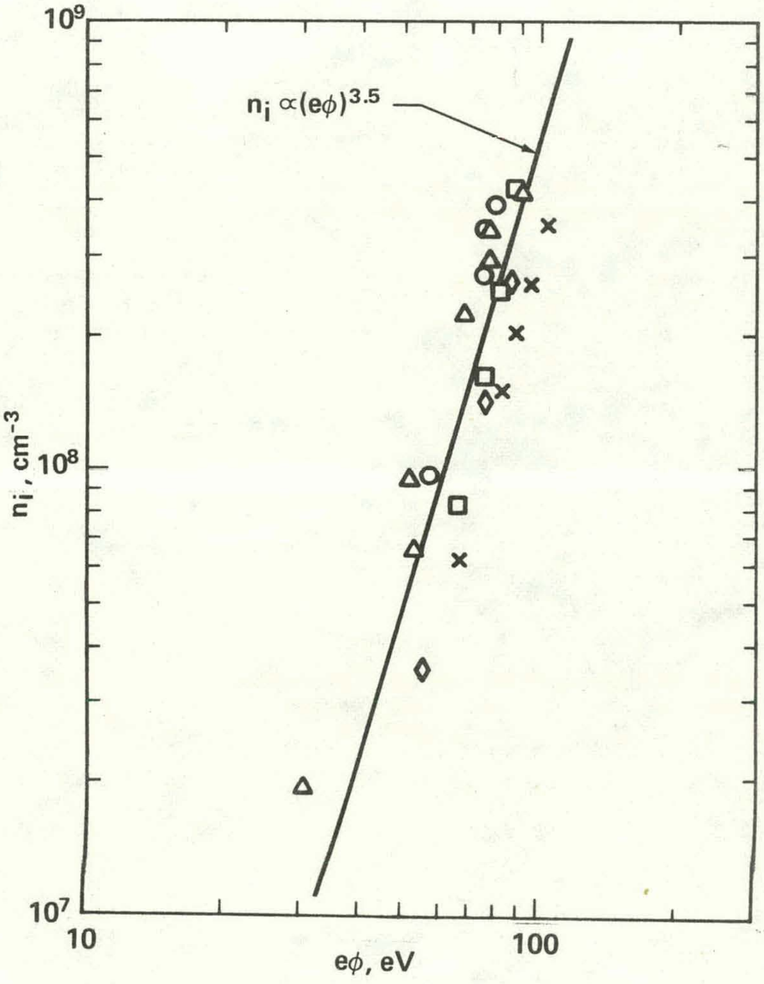

Fig. 5. All published BBI threshold measurements and general sample of BBII results. A fit similar to that in Fig. 4 is shown.

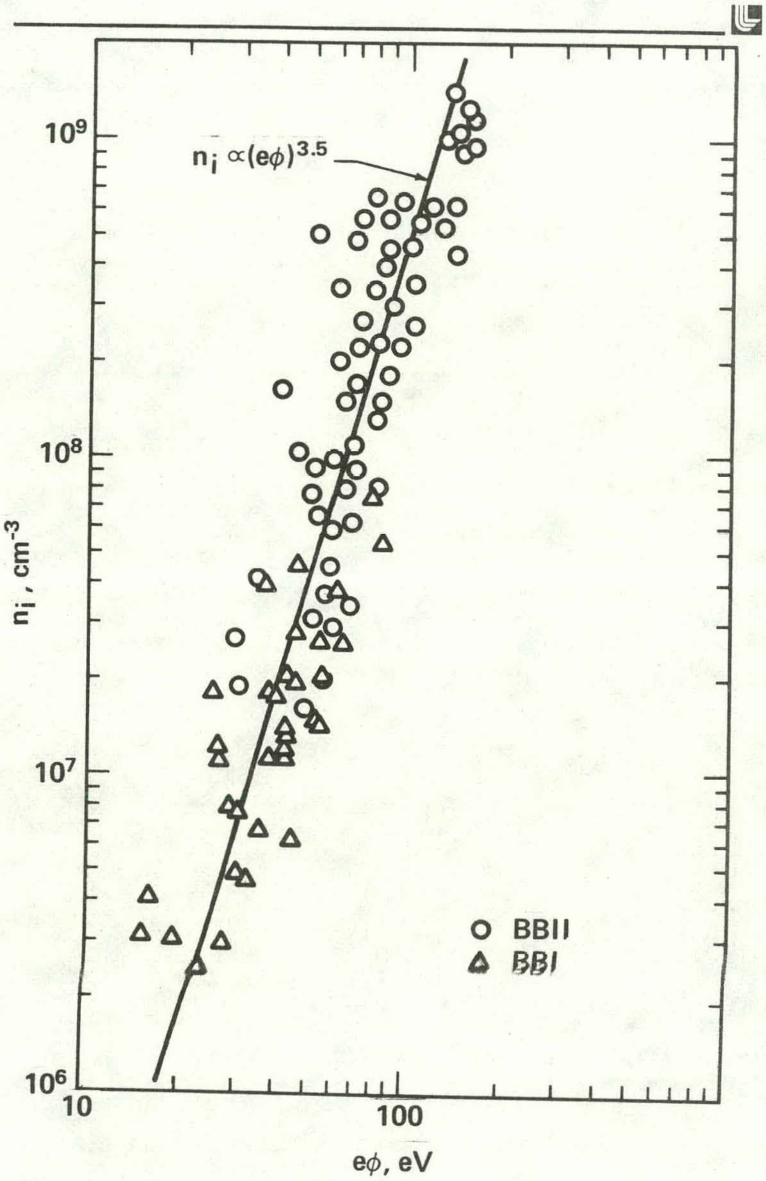

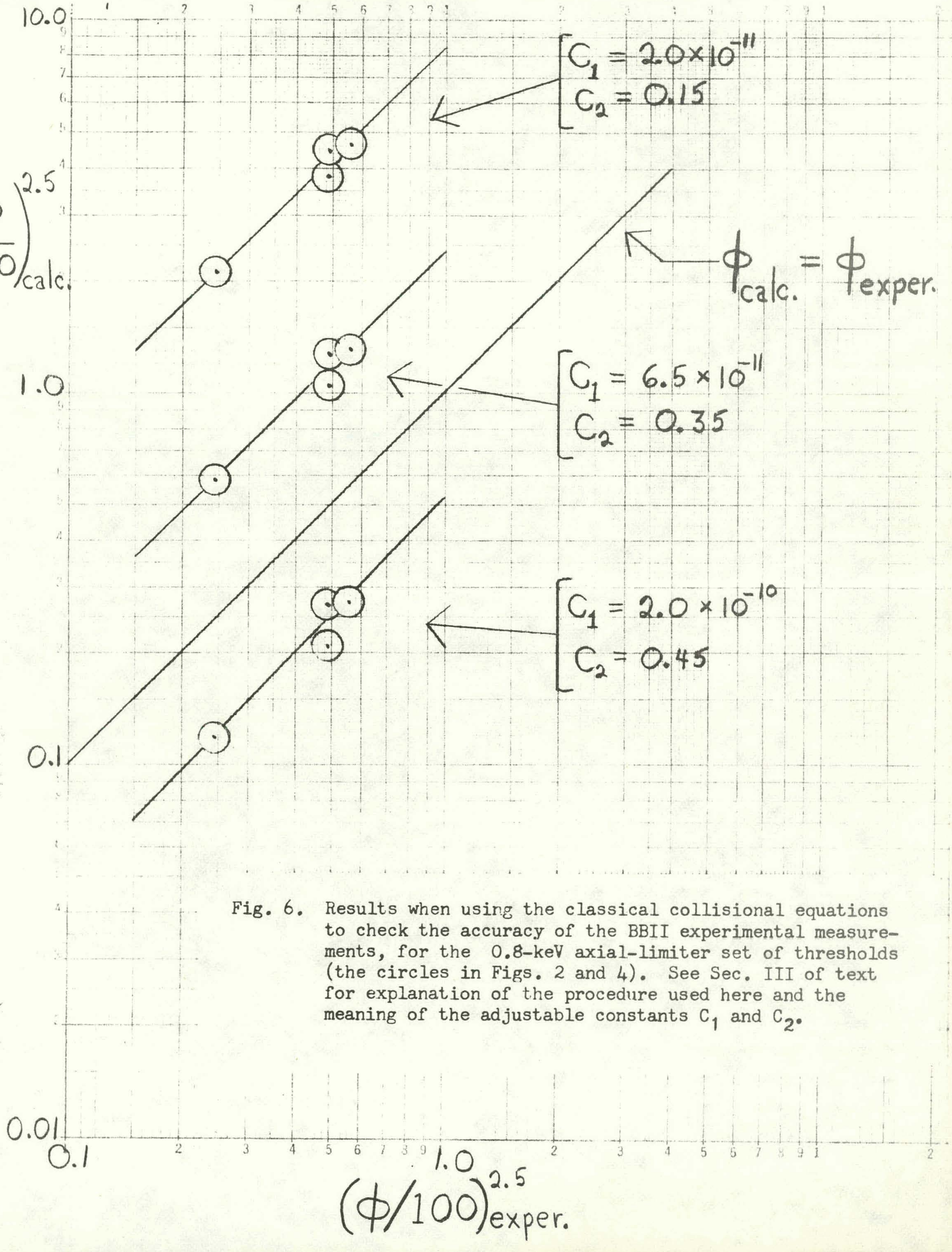

Fig. 6. Results when using the classical collisional equations to check the accuracy of the BBII experimental measurements, for the 0.8-keV axial-limiter set of thresholds (the circles in Figs. 2 and 4). See Sec. III of text for explanation of the procedure used here and the meaning of the adjustable constants C_1 and C_2.

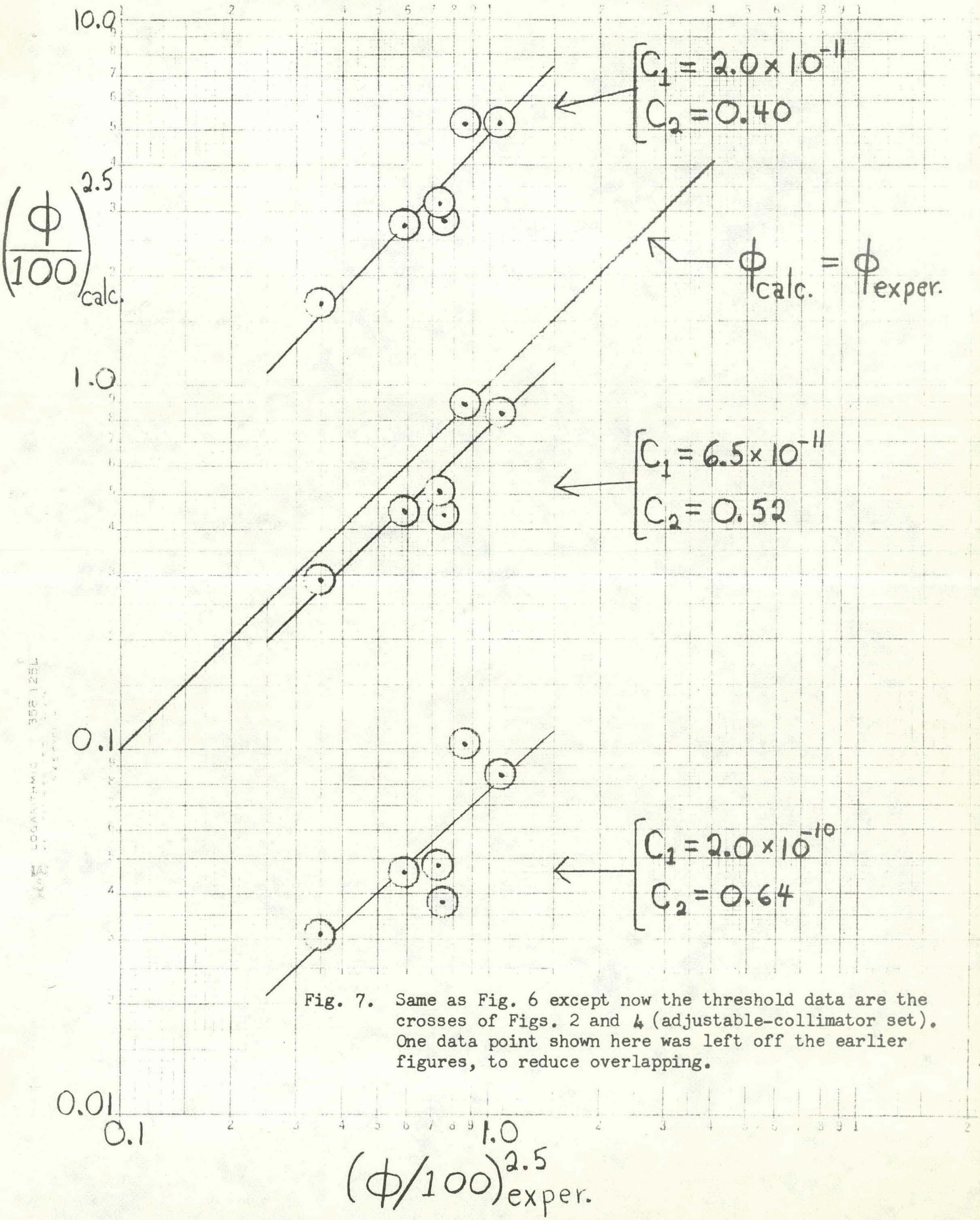

Fig. 7. Same as Fig. 6 except now the threshold data are the crosses of Figs. 2 and 4 (adjustable-collimator set). One data point shown here was left off the earlier figures, to reduce overlapping.

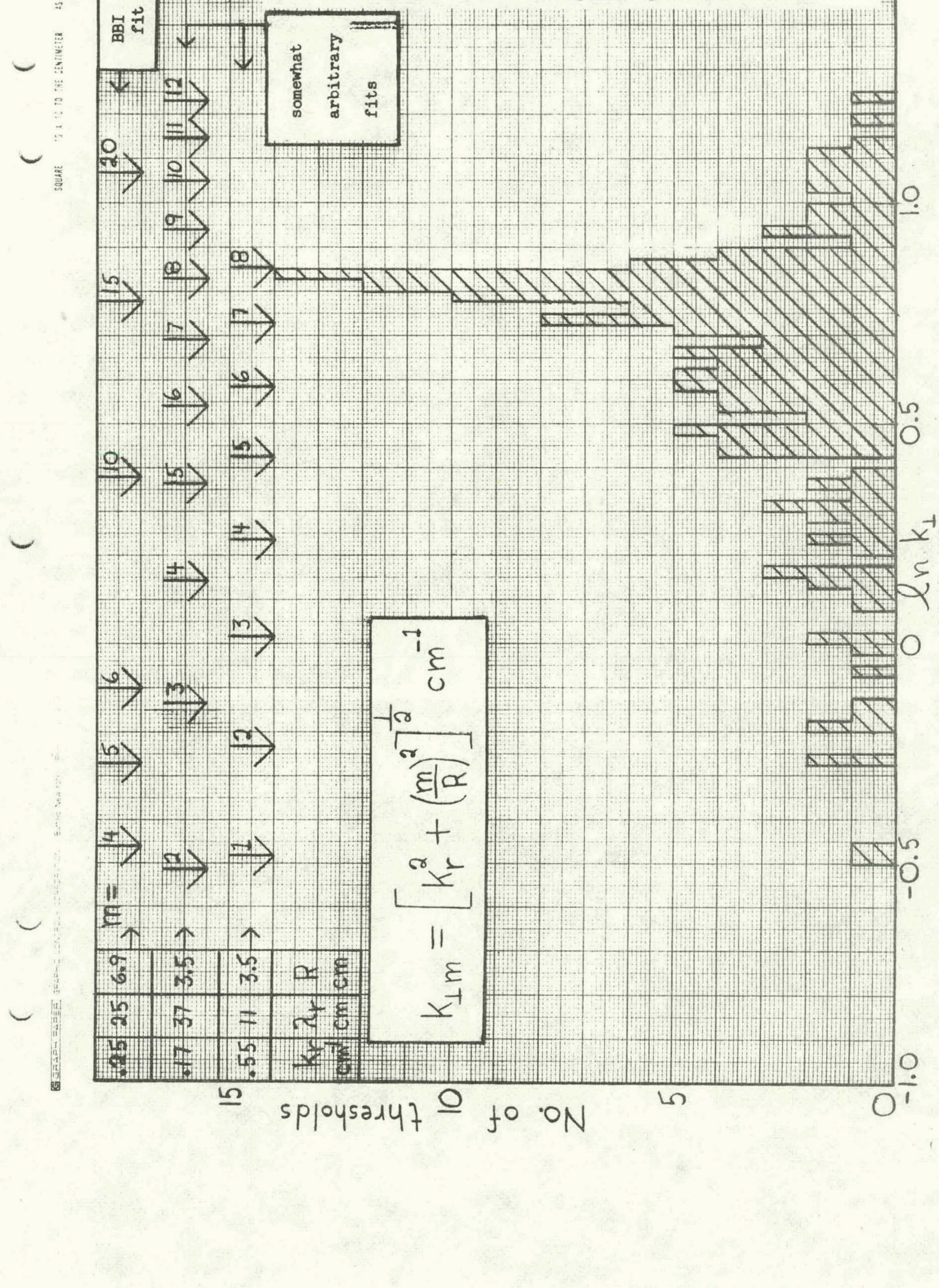

Fig. 8. Histogram showing the number of BBII threshold measurements in each 0.025 interval of ln $k_\perp$ ($k_\perp$ in cm^{-1}). Arrows indicate values of ln $k_{\perp m}$ calculated from the equation given in this figure.

Fig. 9. Plot of $k_\perp$ vs a_i for the BBI and BBII threshold data. The BBI points are noted. (The straight line is a first-order, least-squares fit.)

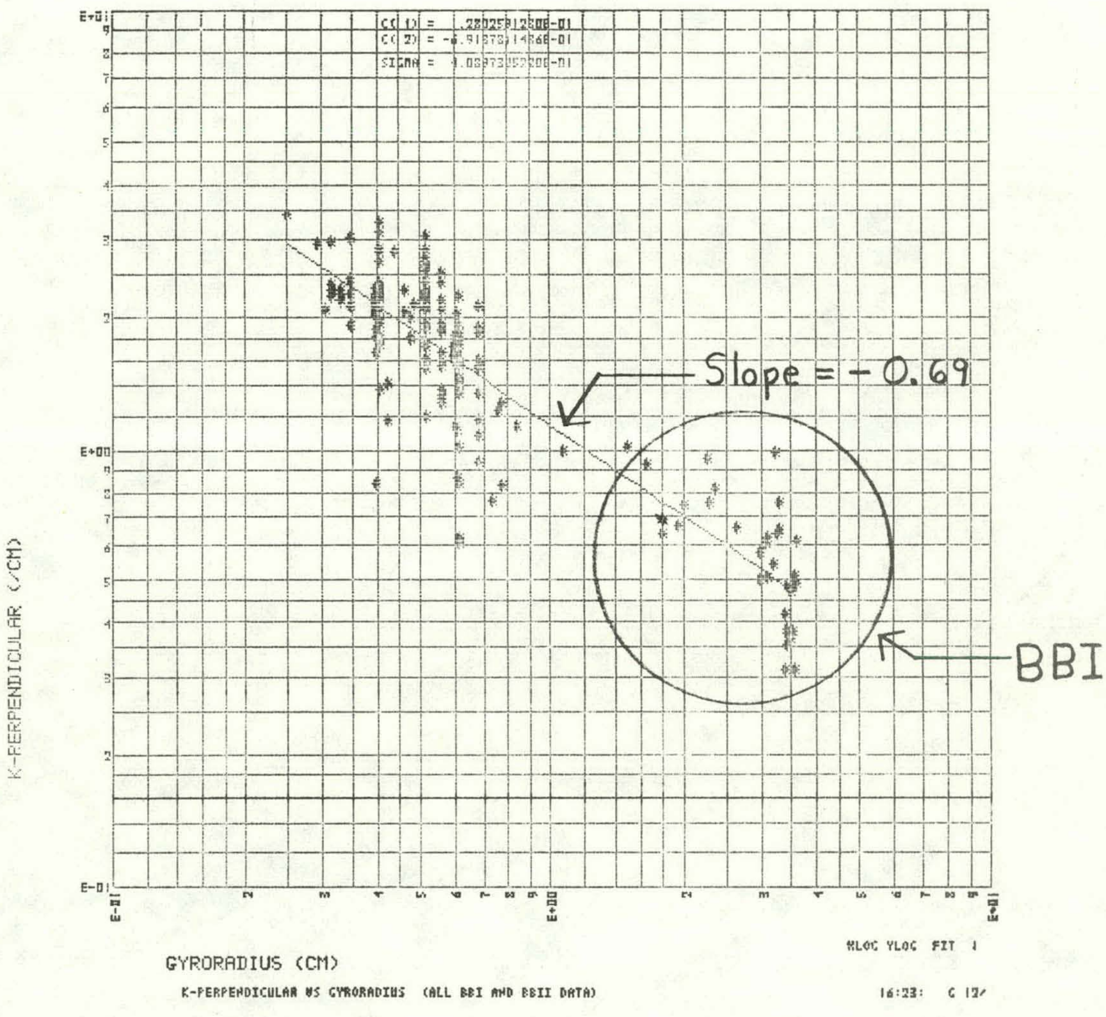

Fig. 10. Plot of $k_{\parallel}$ vs $k_{\perp}$ for the BBI and BBII threshold data. The BBI points are noted. The two BBII points grouped in with the BBI results are the only two BBII threshold measurements in Table I for D^+ instead of H^+. (The first-order, least-squares fit automatically made by the data-reduction program is not too meaningful here.)

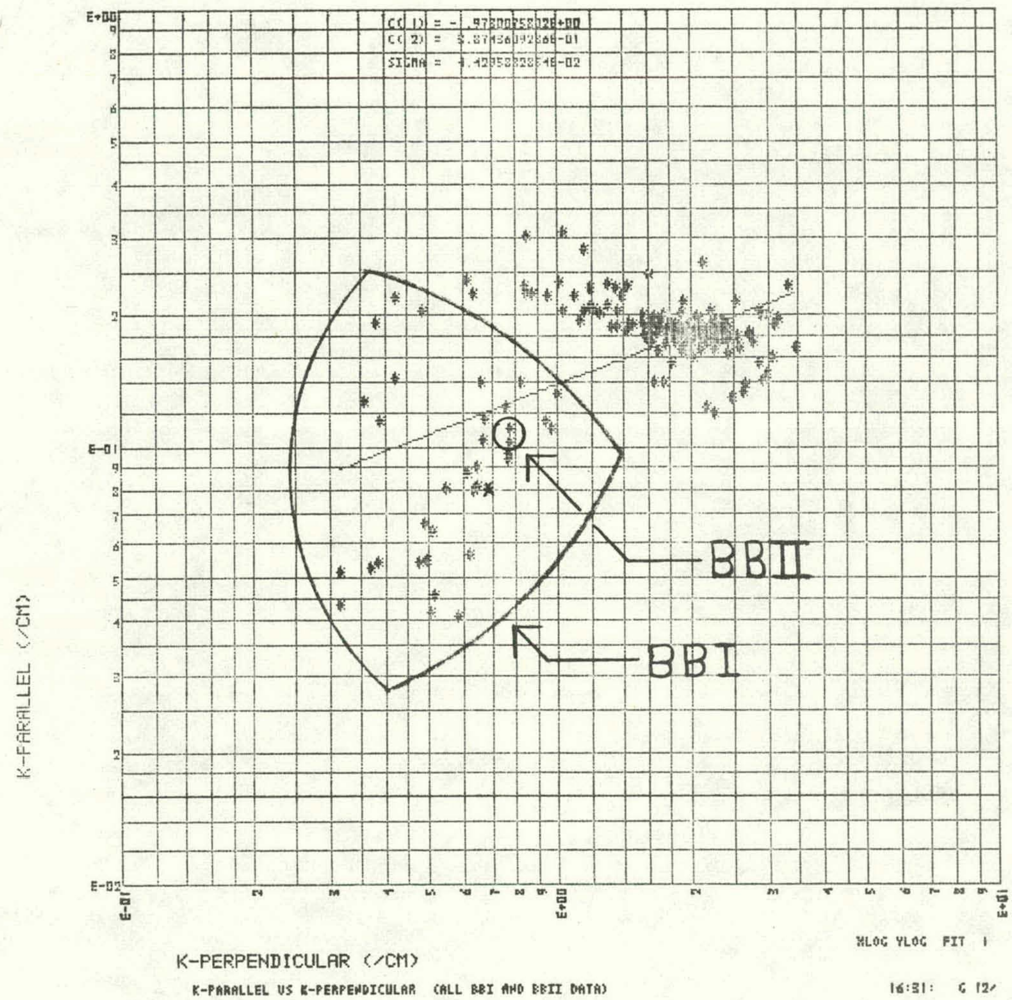

DISTRIBUTION

LLL Internal Distribution		
T.K. Fowler	L-382	
R.F. Post	L-386	
C.E. Taylor	L-386	
F.H. Coensgen	L-382	
M.A. Harrison	L-386	
C.C. Damm	L-386	
A.H. Futch	L-386	
R.K. Goodman	L-386	
G.W. Hamilton	L-386	
A.L. Hunt	L-386	
J.E. Osher	L-386	
G.D. Porter	L-386	
R.W. Moir	L-386	
T.C. Simonen	L-386	
D.E. Baldwin	L-388	
H.L. Berk	L-388	
L.S. Hall	L-388	
B. McNamara	L-388	
N. Maron	L-382	
L.D. Pearlstein	L-388	
J.H. Foote	L-386	(12)
T.I.D.	L-9	(3)

External Distribution

Stephen O. Dean
F. Robert Scott
Division of Controlled Thermonuclear Research
U.S. A.E.C.
Washington, D.C. 20545

Dimitri Panov
Kurchatov Institute of Atomic Energy
46 Ulitsa Kurchatova
Post Box 3402
Moscow, U.S.S.R.

Carl E. Nielsen
Ohio State University
Department of Physics
174 West 18th Avenue
Columbus, Ohio 43210

Ernest Thompson
Culham Laboratory ES/125
Culham, Abingdon, Berkshire
England

Helaman Rolfe Pratt Ferguson
314 TMSB, Depart. of Math
Brigham Young University
Provo, Utah 84602

A.E.C. Technical Information Center (2)